FDTD Analysis of Probe-Fed Cylindrical Dielectric Resonator Antenna

Shiu-Ming Shum and Kwai-Man Luk, *Senior Member, IEEE*

***Abstract*— In this paper, the finite-difference time-domain (FDTD) method is employed to analyze a probe-fed cylindrical dielectric resonator antenna. Numerical results for the input impedance and radiation patterns of the dielectric resonator (DR) antenna operating in $HEM_{11\delta}$ mode are presented and compare favorably with measurements. The effects of various parameters on the characteristics of the DR antenna are studied. Fabrication imperfection effects and the cross-polarization characteristics of this type of DR antenna are also investigated for the first time.**

***Index Terms*—Dielectric antennas, FDTD methods.**

I. Introduction

A CYLINDRICAL dielectric resonator (DR) excited by penetrating a coaxial probe inside its body is an antenna structure proposed by Long [1]. The geometry of the DR antenna is shown in Fig. 1. Only recently, this type of antenna has been analyzed rigorously by a method of moment (MoM) procedure based on the surface integral equation formulation for the bodies of revolution coupled to arbitrary objects [2]. However, when this method is applied to more complex configurations, e.g., stacked cylindrical DR antennas or rectangular DR antennas, the process may become very complicated and time consuming. In addition, the analysis presented in [2] cannot be used to evaluate the fabrication imperfections.

Here, the three-dimensional (3-D) finite-difference time-domain (FDTD) method in rectangular coordinates (Yee cell [3]) is applied to study a probe-fed DR antenna operating at the $HEM_{11\delta}$ mode, which is a broadside mode [1]. The FDTD method in cylindrical coordinates [4] is not suitable for this case with an offset feed (Fig. 1). Compared to the MoM used in [2], the FDTD method is capable of modeling more complicated structures with a relatively simple procedure. The major drawbacks of the FDTD method are the relatively high requirements of both computational and storage resources. However, as the processing power of both PC's and workstations is increasing at such a tremendous rate, this limitation is becoming insignificant.

Efficient theoretical models for the coaxial feed are presented and are used to calculate the input impedance of the antenna. Thereafter, the method used to obtain the radiation patterns of the DR antenna are described.

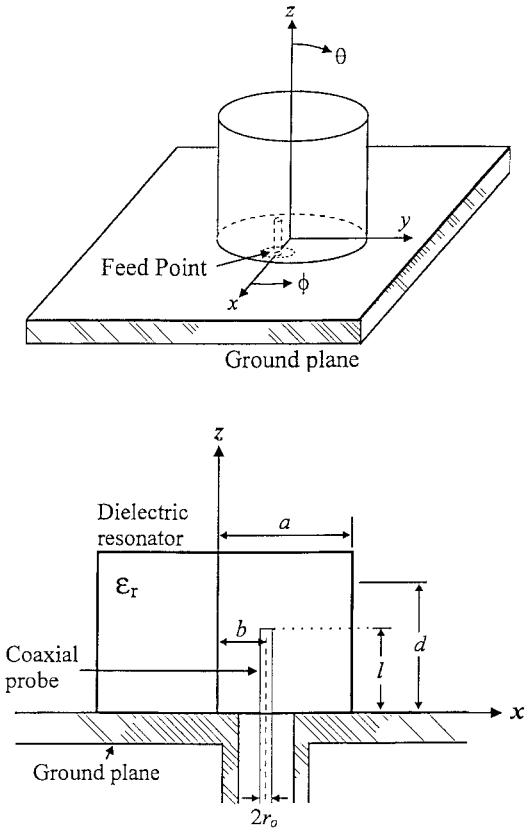

Fig. 1. Geometry of the probe-fed cylindrical DR antenna.

Representative numerical results of the input impedance of a cylindrical DR antenna operating at the $HEM_{11\delta}$ mode are presented. The effects of various parameters on the input impedance are illustrated. The effect of imperfect antenna fabrication on the input impedance is also discussed. Some experimental results are presented to support the numerical computation. Then, the results for the far-fields of the DR antenna are illustrated and verified by measurements taken in a compact antenna test range. The effects of various parameters on the radiation patterns are investigated. Conditions for achieving a minimum cross-polarization level are also discussed.

II. Theory

The FDTD algorithm is well known and is described elsewhere. Details may be referred to in [5] and [6]. As the

Manuscript received August 14, 1996; revised October 1, 1997. This work was supported by the RGC Earmarked Grant 9040165 and the City University Strategic Research Grant.

S.-M. Shum is with the R&D Department, Nirvana Technology Ltd., Hong Kong, China.

K.-M. Luk is with the Department of Electronic Engineering, City University of Hong Kong, Kowloon, Hong Kong, China.

Publisher Item Identifier S 0018-926X(98)02266-2.

second-order Liao absorbing boundary condition (ABC) [7] is easily stabilized, it is used in the present study.

A. Antenna Feed Modeling

Detailed modeling of the coaxial probe is straight forward in the FDTD method. However, as the radius of the coaxial probe feeding the DR antenna is usually much smaller than the radius of the DR, the space steps become very small. The time step will be also very small due to the stability condition. As a result, a large amount of computer memory is required and the computational time is lengthened dramatically.

Alternatively, simplified feed models using thin-wire approximation techniques can be used [8]–[10]. Two simple models include the gap-voltage model and the magnetic-frill model [8]. The excitation schemes of both models are considered as "hard" in the sense of enforcing the fields at some locations to be certain values and neglecting the presence of any reflected waves. Since the reflected waves cannot be absorbed by the source, they are reflected back into the structure under analysis. As a result, the dying down of the response becomes slower and the computation time is lengthened.

Amount the "soft" sources available in the literature, the feed model proposed by Jensen [11], is used in this paper. In this model, the coaxial line connecting the feeding probe is also simulated as shown in Fig. 2. A gap voltage is introduced inside the coaxial cable and the usual FDTD equations are used to propagate the fields toward the antenna. The other end of the coaxial line is terminated by applying an ABC. Any reflected wave from the antenna can now go through the coaxial line and be absorbed. This model has an advantage of determining the input impedance at any point within the coaxial line. From the authors' experience, the required computation time can be as little as 50% of that of the models using "hard" sources. Similar thin wire approximations are also used to calculate the magnetic fields around the coaxial probe. For H_x next to the probe, we have

$$\begin{aligned} H_x^{n+0.5}(i,j,k) = {} & H_x^{n-0.5}(i,j,k) \\ & + \frac{\Delta t}{\mu \Delta z}\left[E_y^n(i,j,k) - E_y^n(i,j.k-1) \right. \\ & \left. \cdot \frac{r_b}{\Delta y}\frac{\ln(r_b/r_a)}{\ln(\Delta y/r_a)}\right] \\ & - \frac{2\Delta t}{\mu \Delta y \ \ln(\Delta y/r_a)} \\ & \cdot [E_z^n(i,j,k) - E_z^n(i,j-1.k)] \end{aligned} \tag{1}$$

where r_a and r_b are the radii of the inner and outer conductors of the coax, respectively.

It should be noted that Jensen's model can only be applied when the radius of the outer conductor of the coax is less than the size of one cell in the antenna region. In fact, all models described here assume the coaxial probe is thin. To model thick probes relative to the size of the space step, conventional FDTD can be used. The computed input impedances obtained by using these antenna feed models are presented and compared in a later section.

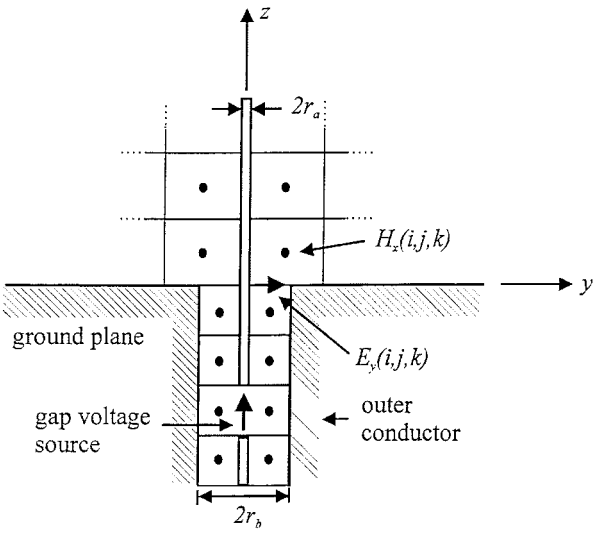

Fig. 2. The Jensen antenna feed model.

B. Input Impedance Calculation

The excitation to the antenna is in the form of a Gaussian pulse

$$V_s(n\Delta t) = e^{-(n\Delta t - t_o)^2/T^2} \tag{2}$$

where T denotes the pulse width and is chosen to cover the frequency range of interest and t_o is the time delay which enables a smooth "turn on" of the pulse. If the voltage-gap antenna-feed model is used, the voltage in (2) is the final one which enters into the input-impedance calculation. If the simulation of the coaxial line is also included, the feed-point voltage can be calculated using the following equation [11]:

$$V_s(n\Delta t) = \frac{r_b}{2}\ \ln\left(\frac{r_b}{r_a}\right) E_y^n(i,j,k-1) \tag{3}$$

where r_a and r_b are the radii of the coax inner and outer conductors, respectively.

The current flowing into the antenna is obtained by performing the line integral of the magnetic fields around the base of the probe at each time step according to Ampere's Law

$$\begin{aligned} I_s[(n+0.5)\Delta t] = {} & [H_x^{n+0.5}(i,j-1,k) \\ & - H_x^{n+0.5}(i,j,k)]\Delta x \\ & + [H_y^{n+0.5}(i,j,k) \\ & - H_y^{n+0.5}(i-1,j,k)]\Delta y. \end{aligned} \tag{4}$$

The input impedance of the antenna is determined from the ratio of the Fourier transform of the voltage wave and the Fourier transform of the input current wave, i.e.,

$$Z(k\Omega) = \frac{\mathrm{DFT}[V_s(n)]}{\mathrm{DFT}[I_s(n)]} \tag{5}$$

where $k\Omega = f_k \cdot 2\pi = 2k\pi/N\Delta t$ and N is the total number of time steps. Either the direct discrete Fourier transform (DFT) or fast Fourier transform (FFT) can be used for the transform process. FFT is generally more time-efficient than DFT. However, even when the simple DFT is used, the computation time for the transform process is negligible compared to the time spent in the FDTD simulation.

C. Far-Field Calculations

To calculate the far-fields of the DR antenna, the equivalent sources on the virtual surface that encloses the antenna are calculated concurrently with the FDTD simulation using the Goertzel algorithm [12]. This is more efficient then the conventional frequency-domain near-to-far field transformation from the FDTD results. After the frequency-domain equivalent sources are known, the far-fields originated by these equivalent sources $\vec{J}_S$ and $\vec{M}_S$ in an unbounded medium can be computed using the equations of integrals shown in Balanis' book [13, eqs. (12-10)–(12-12)]. These integrals are computed numerically according to the positions and orientations of the faces of the virtual surface.

III. Results and Discussion

A. Input Impedance

The first DR antenna considered has the parameters $\varepsilon_r = 12$, $a = 2.75$ cm, $b = 1.4$ cm, $d = 2.6$ cm, $l = 2$ cm, and $r_o = 0.381$ mm. This is the same DR antenna that has been studied in [2]. Therefore, the numerical results using the FDTD method can be verified by comparing them with published results in [2].

The space steps used in FDTD simulation are $\Delta x = 1.72$ mm, $\Delta y = 1.72$ mm, and $\Delta z = 1.63$ mm. The time step used is $\Delta t = 3.13$ ps, such that the Courant stability condition is satisfied. The pulse parameters are $T = 0.1371$ ns and $t_o = 5T$, so the 3-dB bandwidth of the pulse is about 1.4 GHz. The size of the computational domain is 70 $\Delta x \times$ 70 $\Delta y \times$ 35 Δz. The probe feeding configuration are modeled using the simple voltage-gap approximation. The Liao ABC is used to terminate the computation domain. The distance from the object to the absorbing boundary is about 15 space steps in each direction. The simulation is performed for 20 000 time steps to allow the input response to become approximately zero.

The computed results with the use of the voltage-gap model and the measured results obtained from [2] of the input impedance of the DR antenna are plotted against frequency in Fig. 3. The dominant $\mathrm{HEM}_{11\delta}$ mode of the DR antenna is considered. It can be seen from the figure that the agreement between calculated and measured results is good. The computed resonant frequency is 1.346 GHz whereas the measured resonant frequency from [2] is 1.33 GHz. This gives a percentage error of 1.2%. It should be noted that a conventional DR has not been used in the fabricated antenna used in [2]. The DR antenna was constructed out of a section of PVC tube packed with "Hi K Power." The permittivity of the PVC container is low so that it can be neglected in the computation. The reason for such an experimental arrangement is to ensure that there are no air gaps between the dielectric material and the conducting surfaces. The presence of air gaps can cause the resonant frequency and the input impedance to change dramatically. Theoretical models that do not account for these fabrication imperfections can hardly produce results that compare favorably with measurements. The technique for modeling these fabrication imperfections will be described later.

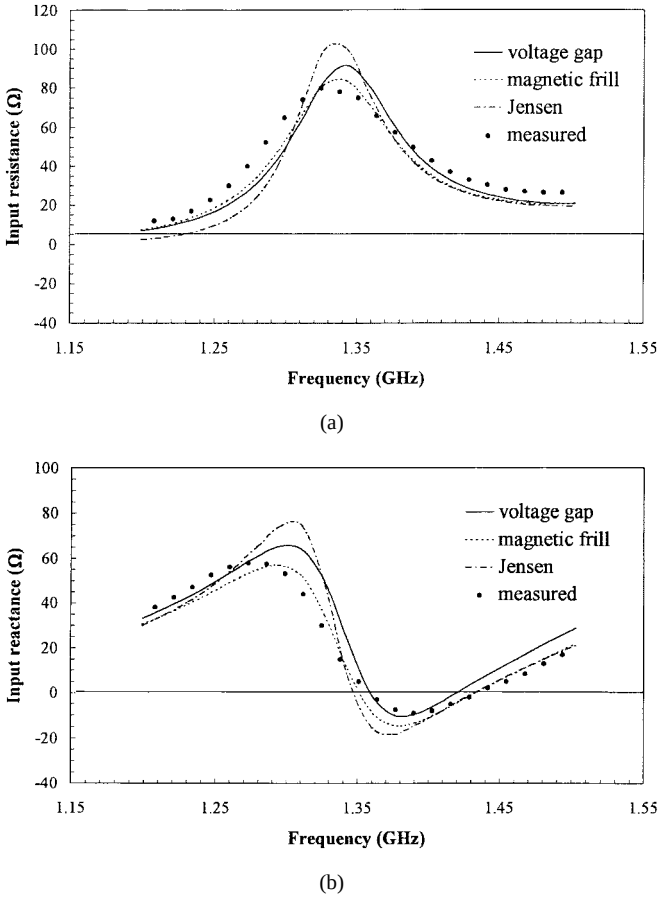

Fig. 3. Input impedance of the DR antenna against frequency for using different types of antenna feed models. (a) Input resistance. (b) Input reactance. $\varepsilon_r = 12$, $a = 2.75$ cm, $b = 1.4$ cm, $d = 2.6$ cm, $l = 2$ cm, and $r_o = 0.381$ mm.

The effect of using different feeding models is now investigated. The calculated input impedance results of using the magnetic frill-like model and Jensen's model are also illustrated in Fig. 3. It can be seen from the figure that the feed models produce only slightly different results in terms of input impedance. The Jensen's feed model gives the largest value of input impedance. However, the computation time can be shortened when using the Jensen's feed model. Fig. 4(a) and (b) shows the computed time-domain current flowing into the DR antenna using the voltage-gap model and Jensen's feed model, respectively. The transient current in the first case decays slowly toward zero and shows apparent oscillations after 20 000 time steps. In the Jensen's feed model case, the input transient current drops quickly and only requires about 10 000 time steps for the time response to die down, so

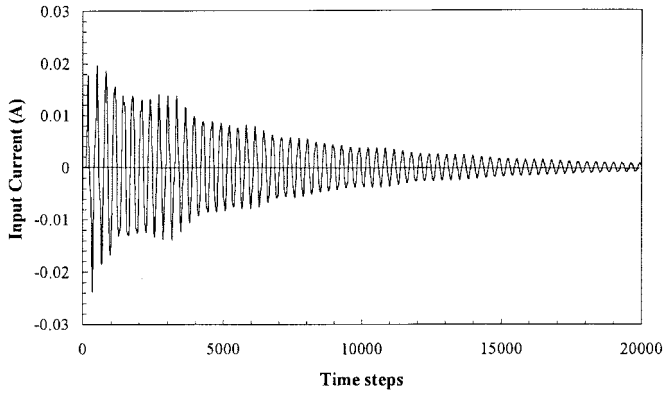

(a)

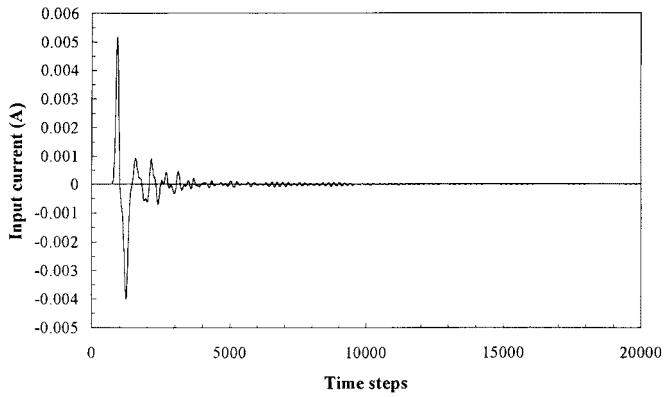

(b)

Fig. 4. Time-domain waveform of input current of the DR antenna against frequency for using different types of antenna feed models. (a) Voltage-gap model. (b) Jensen model. $\varepsilon_r = 12$, $a = 2.75$ cm, $b = 1.4$ cm, $d = 2.6$ cm, $l = 2$ cm, and $r_o - 0.381$ mm.

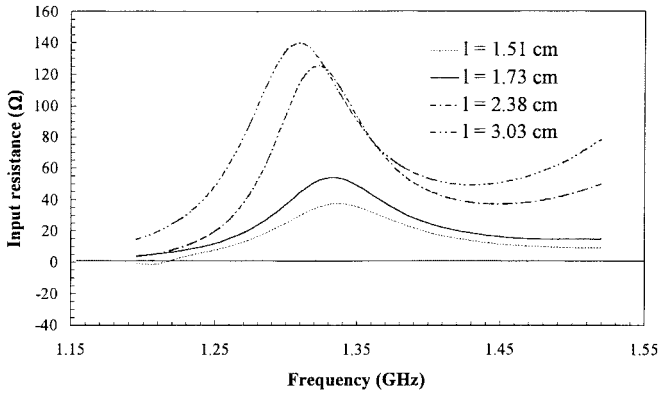

(a)

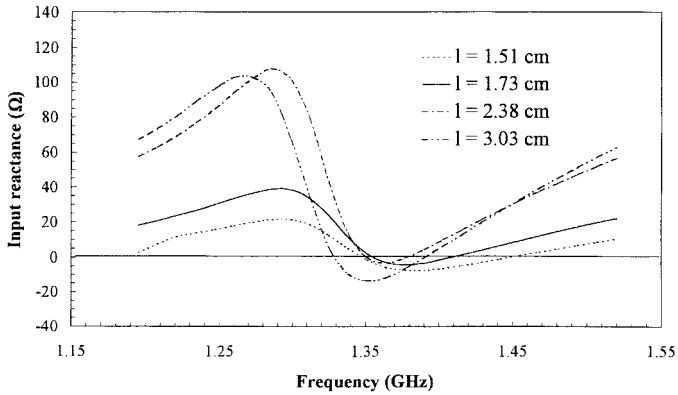

(b)

Fig. 5. Input impedance of the DR antenna against frequency for different probe length l. (a) Input resistance. (b) Input reactance. $\varepsilon_r = 12$, $a = 2.75$ cm, $b = 1.4$ cm, $d = 2.6$ cm, and $r_o = 0.381$ mm.

computation time is greatly saved. Therefore, it is preferable if computing resources are limited. On the other hand, the simple gap-voltage model is the simplest and produces results showing better agreement with measurement. It is used for subsequent calculations.

The effect of varying the probe length is illustrated in Fig. 5. We can see that both the input resistance and impedance increase with the probe length l. This property can be used for impedance matching. On the other hand, the resonant frequency decreases with the probe length. The height of the DR under consideration is 2.6 cm, so the two curves showing the input impedance for $l = 3.03$ cm indicate that the probe is passing through the DR. However, since the input impedance does not change drastically, this is feasible during impedance matching, especially for large ratio of a and d.

Next, the effect of changing probe displacement from the axis of the DR on the input impedance of the antenna is studied. The computed input impedance for different probe displacement b is plotted against frequency in Fig. 6. From this figure, we can see that as b increases, input resistance decreases and the input reactance becomes more capacitive. This parameter can also be used to tune the input impedance of the antenna. For strong coupling of the $\mathrm{HEM}_{11\delta}$ mode, the probe should be located near the edge of the DR. Furthermore, if the probe is placed outside the DR (the curves corresponding to $b = 3$ cm), the impedance becomes highly capacitive, which should normally be avoided.

The effect of the dielectric constant ε_r on the input impedance and the resonant frequency of the DR antenna is studied. The computed input impedance of the DR antenna for different ε_r is shown in Fig. 7. As shown in the figure, as ε_r is increased, the resonant frequency decreases and the value of the input impedance increases. The input impedance also becomes more inductive if ε_r is decreased.

For studying the effect of ε_r on the impedance bandwidth of the antenna, the feed position b and the length of the probe are initially adjusted to match the input impedance of the antenna to 50 Ω. The computed results on the return loss of the antenna for different ε_r are shown in Fig. 8. It is observed that the impedance bandwidth (return loss $>$ 10 dB) increases when ε_r is decreased. The computed impedance bandwidths for $\varepsilon_r = 9.8$, 12, and 16 are 9.3, 8.8, and 7.6%, respectively.

The general procedure for matching a probe-fed cylindrical DR antenna can be inferred from the examination of Figs. 5–8. First, the position of probe b should be adjusted to tune the input reactance of the DR antenna to zero, at the resonant frequency. After this is accomplished, the probe length l is adjusted to tune the input resistance to 50 Ω. For a DR with

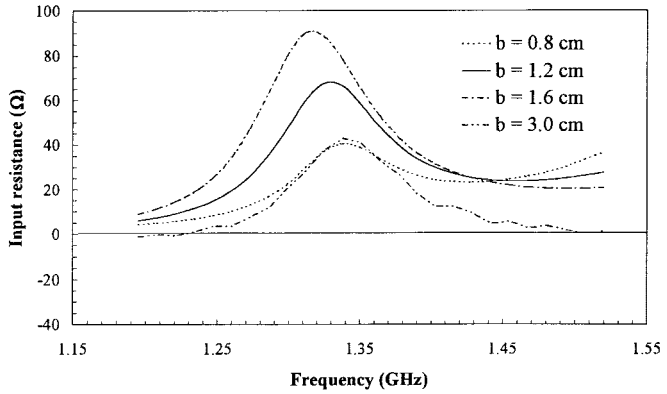

(a)

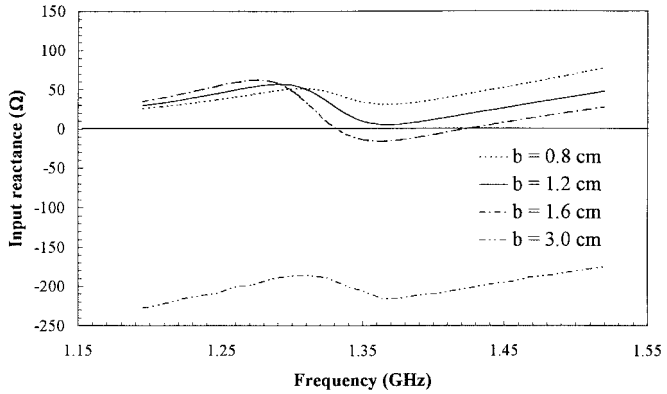

(b)

Fig. 6. Input impedance of the DR antenna against frequency for different probe displacement b. (a) Input resistance. (b) Input reactance. $\varepsilon_r = 12$, $a = 2.75$ cm, $d = 2.6$ cm, $l = 2$ cm, and $r_o = 0381$ mm.

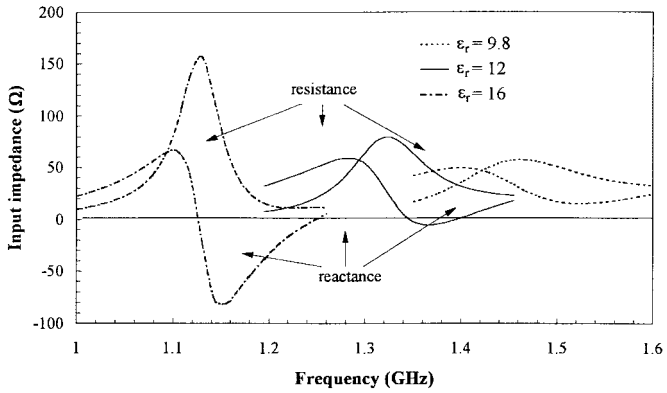

Fig. 7. Computed input impedance of the DR antenna against frequency for different ε_r. $a = 2.75$ cm, $b = 1.4$ cm, $d = 2.6$ cm, and $l = 2$ cm.

high ε_r, the desirable probe position will be closer to the axis of the DR and the impedance bandwidth is relatively narrow. Later, we will see that it is preferred to have the position of the probe closer to the edge of the DR for lower cross-polarization. Hence, for better performance of the antenna, DR with smaller ε_r should be used in constructing the antenna.

B. Effect of Fabrication Imperfections on the Input Impedance

Besides comparing the computed results to published measured results, independent experiments have also been performed. The DR used for the experiment has the parameters $\varepsilon_r = 9.2$, $a = 6.1$ mm, $b = 4.15$ mm, $d = 12.2$ cm, and $l = 5.1$ mm. The radius of the probe r_o is 0.51 mm. The voltage-gap antenna model is used initially in the FDTD simulation to calculate the input impedance of the antenna. The space steps used in the FDTD computation are $\Delta x = 0.488$ mm, $\Delta y = 0.488$ mm, and $\Delta z = 0.470$ mm, and the time step used is $\Delta t = 0.9$ ps. The size of the computational domain is 40 $\Delta x \times$ 40 $\Delta y \times$ 30 Δz. The input impedance of the fabricated antenna is measured using a HP8510C Network Analyzer. The calculated results and the measured results of the input impedance of the DR antenna are plotted against frequency in Fig. 9. It can be seen from the figure that large discrepancies are observed between the calculated and measured results on the resonant frequency and the value of the input impedance.

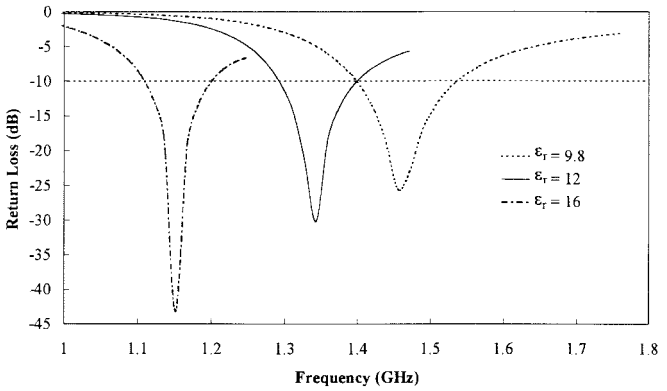

Fig. 8. Computed return losses of the DR antenna against frequency for different ε_r. $\varepsilon_r = 9.8$, $a = 2.75$ cm, $b = 2.0$ cm, $d = 2.6$ cm, and $l = 1.8$ mm. $\varepsilon_r = 12$, $a = 2.75$ cm, $b = 1.6$ cm, $d = 2.6$ cm, and $l = 1.7$ mm. $\varepsilon_r = 16$, $a = 2.75$ cm, $b = 1.4$ cm, $d = 2.6$ cm, and $l = 1.5$ mm.

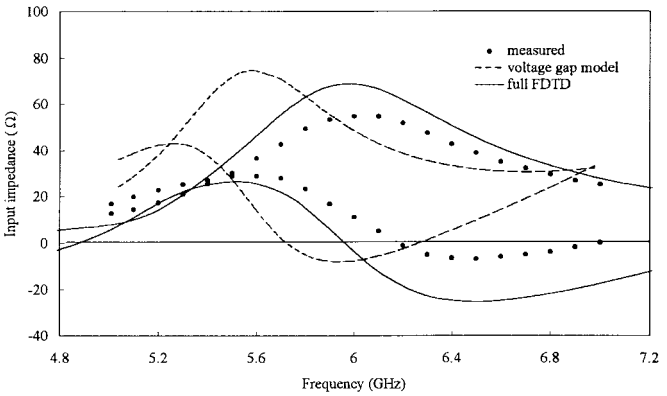

Fig. 9. Computed and measured input impedance for the DR antenna against frequency. $\varepsilon_r = 9.8$, $a = 6.1$ mm, $b = 4.15$ cm, $d = 12.2$ mm, $l = 5.1$ mm, $r_o = 0.51$ mm.

Since a conventional DR is used in the experiment, a hole is drilled into the DR for probe accommodation. This creates a small air gap t_p between the probe and the body of the DR. Furthermore, an air gap t_g also exists between the ground plane and the DR due to imperfect physical contact. The revised antenna geometry showing these fabrication imperfections is shown in Fig. 10. The air gaps introduce discontinuities in

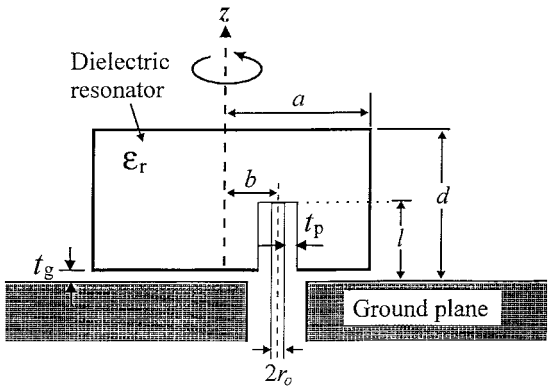

Fig. 10. Geometry of the probe fed cylindrical DR antenna including the fabrication imperfections.

the normal component of the electric fields at the dielectric-air interfaces. As a result, the measured resonant frequency and the value of the input impedance may shift significantly from the ideal case because the associated near fields are changed. This is the reason why the computed results using the simple antenna feed model cannot predict accurately the resonant frequency and the value of the input impedance of the fabricated DR antenna. Special arrangements have been made for the experiments performed in [2] to enable favorable comparison against theory. However, conventional DR's will still be used for constructing most of the DR antennas for convenience. Hence, theoretical models, which are capable of including these fabrication imperfections, are useful. No such theoretical model is available thus far to the knowledge of the author. The study of the effect of fabrication imperfections on the antenna characteristics in [14] is mainly experimental. Here, a first attempt is made to simulate a "realistic" DR antenna with fabrication imperfections numerically using the FDTD method.

Incorporating the air gaps into the formulation of the MoM is difficult because of the additional material boundaries. On the other hand, due to the high flexibility of the FDTD method, only redefinition of the locations of the media in the computational space is required. Here, the fabrication imperfections are modeled by adding air layers between the probe and the DR and also between the ground plane and the DR. The thickness of each air layer is set to the size of one space step. The space steps used in the FDTD computation are $\Delta x = 0.244$ mm, $\Delta y = 0.244$ mm, and $\Delta z = 0.235$ mm and the time step used is $\Delta t = 0.45$ ps. The size of the new computational domain is 80 $\Delta x \times$ 80 $\Delta y \times$ 65 Δz. The calculated results using the new model and the measured results of the input impedance of the DR antenna are also plotted in Fig. 9. It can be seen from the figure that the agreement between the calculated and measured results is reasonable. The discrepancy between the two results is caused by the staircase approximations of the air gap in the numerical model.

The effect of the air-gap thickness t_g on the input impedance is studied by adjusting the thickness of the air gap in the FDTD program. The numerical results for three different t_g (with $t_p = 0$) are illustrated in Fig. 11. We can see from the figure that the resonant frequency increases with t_g, but the value of the input impedance decreases with t_g. The resonant frequency in case of $t_g = 0.24$ mm shifts by 5% from the ideal case of no air gap. Doubling the air-gap thickness t_g from 0.48 to 0.96 mm causes a similar percentage shift in the resonant frequency.

The effects of the air-gap thickness t_p on the input impedance are also studied and the numerical results for three different t_p (with $t_g = 0$) are also shown in Fig. 11. It is observed that increasing t_p causes the resonant frequency to increase, but the change is not as large as in the case of increasing t_g. The case of $t_p = 0.24$ mm causes only a small change in the resonant frequency whereas doubling t_p from 0.48 to 0.96 mm causes a 2% shift in the resonant frequency. The value of the input impedance increases slightly with t_p, the air gap around the coaxial probe.

It can be concluded that the incorporation of fabrication imperfections in the theoretical model is essential for accurate calculation of the resonant frequency and the value of the input impedance of the probe-fed DR antenna.

C. Far-Fields

The DR antenna considered has parameters: $\varepsilon_r = 9.2$, $a = 6.1$ mm, $b = 4.15$ cm, $d = 12.2$ mm, and $l = 5.1$ mm. The radiation patterns of the fabricated antenna are measured in an anechoic chamber using a HP85310C Antenna Measurement System. The size of the ground plane of the fabricated antenna is 6 $\lambda_o \times$ 6 λ_o, where λ_o is the free-space wavelength at the resonant frequency. Both the calculated and measured radiation patterns of the antenna are shown in Fig. 12. It can be seen from the figure that the agreement between the results is quite good. The discrepancies are mainly due to the infinite ground plane assumption used in the calculation. The radiation pattern of the DR antenna is similar to that of a magnetic dipole. The asymmetry of the E-plane radiation pattern is due to presence of higher order modes. Furthermore, Fig. 12 shows that the H-plane cross polarization of the antenna is less than 10 dB, which may be unsatisfactory.

Next, the effect of changing the probe position on the radiation patterns of the antenna is investigated. The dimensions of the antenna are unchanged and the distance of the probe from the center of the DR, b is varied between $0.2a$ and $0.9a$. For each value of b, the probe length is adjusted to maintain impedance matching. The results on the radiation patterns for three different values of b/a are plotted in Fig. 13(a)–(c). From these figures, it can be seen that as b is increased, both the cross polarization and the asymmetry of the E-plane pattern is reduced. Hence, the feeding probe should be located as close to the edge of the DR as possible. It is worth noting that the resonant frequency of the antenna only changes slightly when the probe position is changed.

The effect of changing the ratio of the radius and the height of the DR is also studied. The radiation patterns for three different values of a/d are plotted in Fig. 14(a) and (b). Again, Fig. 14(c) for each value of a/d, the probe length is adjusted to maintain impedance matching. From these figures, it is observed that small values of a/d produce smaller cross-

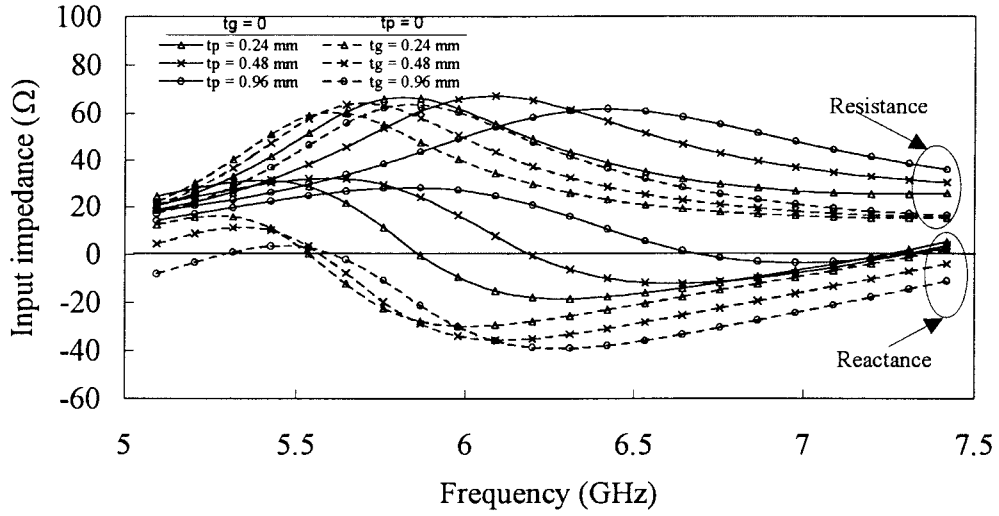

Fig. 11. Computed input impedance versus frequency for different air-gap thickness t_p and t_g. $\varepsilon_r = 9.8$,$a = 6.1$ mm, $b = 4.15$ cm, $d = 12.2$ mm, $l = 5.1$ mm, and $r_o = 0.51$ mm.

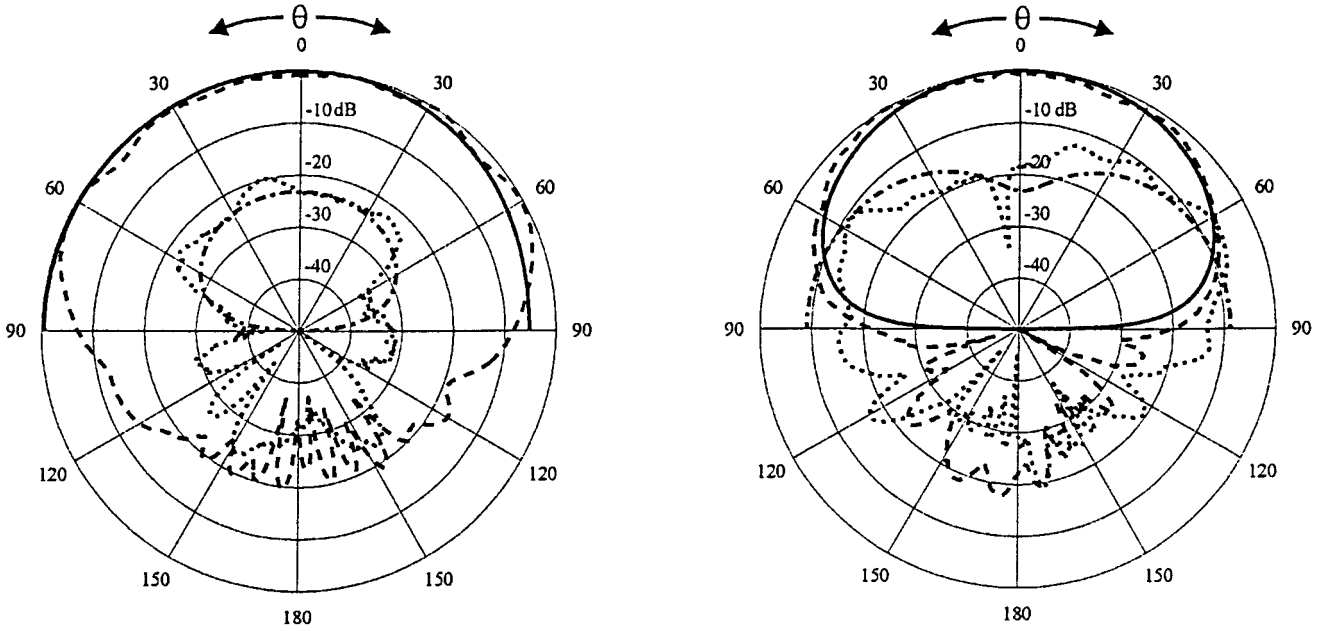

Fig. 12. Calculated and measured radiation patterns for the DR antenna. (a) E-plane. (b) H-plane. ——— copol (computed); - - - - copol (measured); - · - · - · - Xpol (computed); ····· Xpol (measured).

polarized fields. However, if a/d is smaller than 0.2, it may be difficult to match the input impedance of the antenna to 50 Ω. Since a is fixed in the calculations, the resonant frequency increases when a/d is increased.

IV. Conclusions

This paper has presented a numerical method for modeling probe-fed cylindrical DR antennas. The approach is based on the well-known FDTD method: a 3-D algorithm for directly solving Maxwell's equation in the time domain. Numerical results for the input impedance of the DR antenna operating in $\mathrm{HEM}_{11\delta}$ mode were presented. The effects of various parameters on the input impedance of the DR antenna were studied. The impedance matching of the antenna can be accomplished by adjusting the position b and the length l of the coaxial probe. For DR's with low ε_r, b should be slightly smaller than the radius of the DR. It is concluded that a DR with low ε_r (e.g., $\varepsilon_r = 9.8$) is preferred for constructing the antenna due to the wider impedance bandwidth.

The presence of fabrication imperfections in the antenna used in experiments causes the resonant frequency and the value of the input impedance of the antenna to change significantly from the ideal case. In this case, the air gaps between the bottom of the DR and the ground plane and around the coaxial probe are handled using the standard FDTD method.

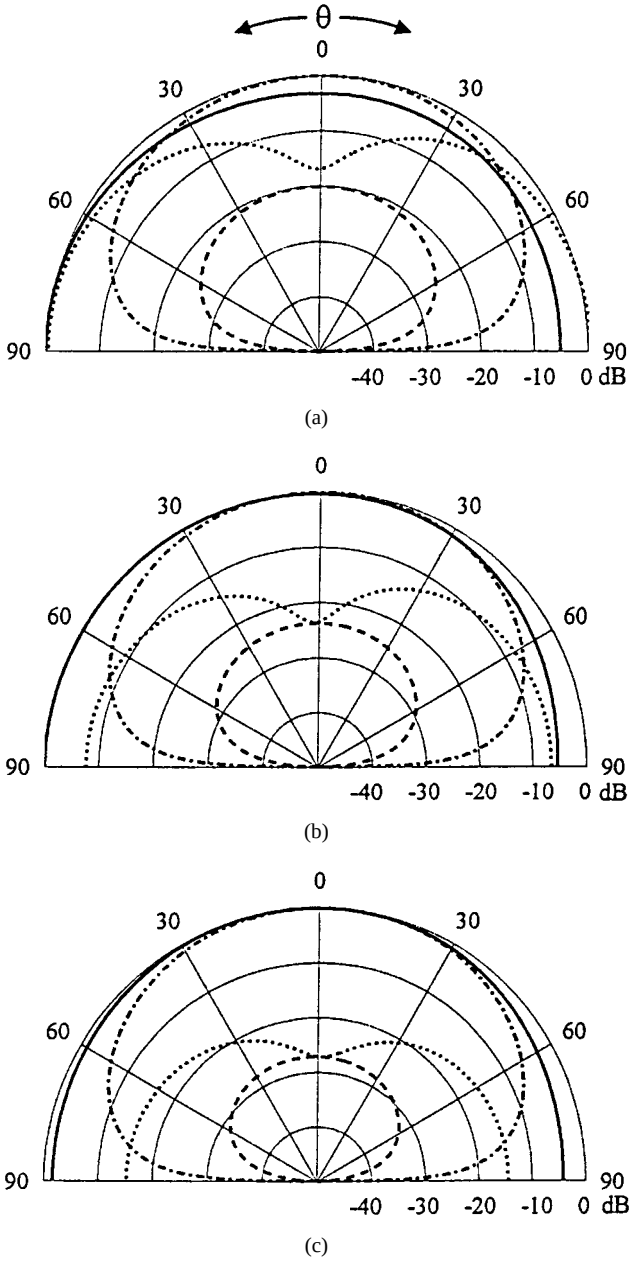

Fig. 13. Far-field patterns for different b/a. $\varepsilon_r = 9.2$, $a = 6.1$ mm, $b = 4.15$ cm, $d = 12.2$ mm, and $l = 5.1$ mm. (a) $b/a = 0.3$. (b) $b/a = 0.6$. (c) $b/a = 0.9$. ——— E-plane copol. - - - - E-plane Xpol. - - - - - - - H-plane copol. ····· H-plane Xpol.

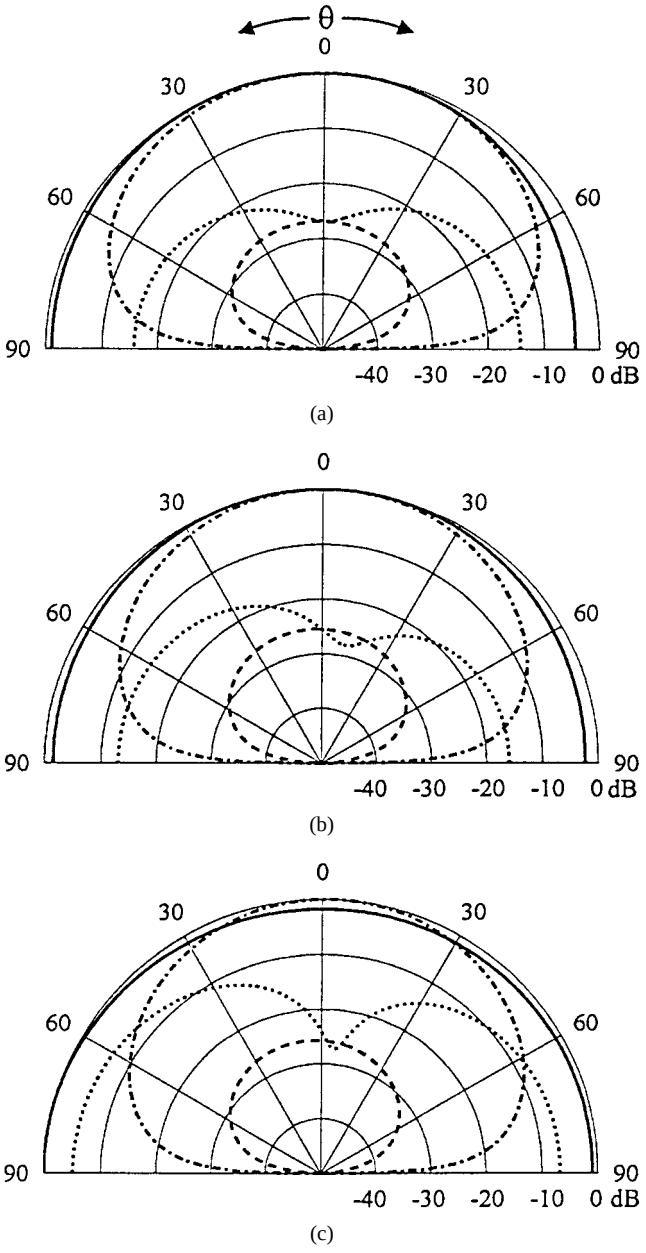

Fig. 14. Far-field patterns for different a/d. $\varepsilon_r = 9.2$, $a = 6.1$ mm, $b = 4.15$ cm, $d = 12.2$ mm, and $l = 5.1$ mm. (a) $a/d = 0.4$. (b) $a/d = 1.0$. (c) $a/d = 1.6$. ——— E-plane copol. - - - - E-plane Xpol. - - - - - - - H-plane copol. ····· H-plane Xpol.

The resonant frequency computed in this way agrees well with the measured data.

Finally, the numerical results on the far fields of the DR antenna were presented. The computed results are consistent with measured results. The DR radiates like a magnetic dipole when operating in the $\mathrm{HEM}_{11\delta}$ mode. The cross polarization attains a maximum at $\phi = 45°$ and $\phi = 135°$. It is found that to achieve a low cross polarization, the feeding probe should be located near the edge of the DR and the ratio of the radius to the height of the DR antenna should be kept small. The condition again suggests that a DR with low ε_r should be used to ease impedance matching.

REFERENCES

[1] S. A. Long, M. W. Mcallister, and L. C. Shen, "The resonant cylindrical dielectric cavity antenna," *IEEE Trans. Antennas Propagat.*, vol. AP-31, pp. 406–412, May 1983.

[2] G. P. Junker, A. A. Kishk, and A. W. Glisson, "Input impedance of dielectric resonator antennas excited by a coaxial probe," *IEEE Trans. Antennas Propagat.*, vol. 42, pp. 960–966, July 1994.

[3] K. S. Yee, "Numerical solution of initial boundary value problems involving Maxwell's equations in isotropic media," *IEEE Trans. Antennas Propagat.*, vol. AP-14, pp. 302–307, May 1966.

[4] J. G. Maloney, G. S. Smith, and W. R. Scott, Jr., "Accurate computation of the radiation from simple antennas using the finite-difference time-domain method," *IEEE Trans. Antennas Propagat.*, vol. 38, pp. 1059–1068, July 1990.

[5] K. S. Kunz and R. J. Luebbers, *The Finite Difference Time Domain Method for Electromagnetics*. Boca Raton, Florida: CRC, 1993.

[6] A. Taflove, *Computational Electrodynamics The Finite-Difference Time-Domain Method*. Norwood, MA: Artech House, 1995.
[7] Z. P. Liao, H. L. Wong, B. P. Yang, and Y. F. Yuan, "A transmitting boundary for transient wave analysis," *Scientia Sinica*, vol. XXVII, ser. A, pp. 1063–1076, 1984.
[8] R. J. Luebbers, L. Chen, T. Uno, and S. Adachi, "FDTD calculation of radiation patterns, impedance, and gain for a monopole antenna on a conducting box," *IEEE Trans. Antennas Propagat.*, vol. 40, pp. 1577–1583, Dec. 1992.
[9] P. A. Tirkas and C. A. Balanis, "Finite difference time domain method for antenna radiation," *IEEE Trans. Antennas Propagat.*, vol. 40, pp. 334–340, Mar. 1992.
[10] A. Taflove and A. R. Umashankar, "Finite difference time domain modeling of electromagnetic wave scattering and interaction problems," *IEEE Antennas Propagat. Soc. Newslett.*, vol. 30, pp. 5–20, Apr. 1988.
[11] M. A. Jensen and Y. Rahmat-Samii, "Performance analysis of antenna for hand-held transceivers using FDTD," *IEEE Trans. Antennas Propagat.*, vol. 42, pp. 1106–1113, Aug. 1994.
[12] A. V. Oppenheim and R. W. Schafer, *Discrete-Time Signal Processing*. Englewood Cliffs, NJ: Prentice-Hall, 1989.
[13] C. A. Balanis, *Antenna Theory-Analysis and Design*. New York: Harper & Row, 1982.
[14] G. P. Junker, A. A. Kishk, A. W. Glisson, and D. Kaifez, "Effect of fabrication imperfections for ground plane backed dielectric resonator," *IEEE Antennas Propagat. Mag.*, vol. 37, pp. 40–46, Feb. 1995.

Shiu-Ming Shum was born in Hong Kong. He received the B.Sc. and Ph.D. degrees in electronic engineering from the City University of Hong Kong, Kowloon, in 1991 and 1996, respectively.

Since January 1997, he has been with the R&D Department, Nirvana Technology Ltd., Hong Kong as a Manager. His research interests include dielectric resonator antennas and numerical method in electromagnetics.

Kwai-Man Luk (S'80–M'86–SM'94) was born in Hong Kong in 1958. He received the B.Sc. (Eng.) and Ph.D. degrees in electrical engineering from the University of Hong Kong, in 1981 and 1985, respectively.

From 1985 to 1987, he was employed as a Lecturer in the Department of Electronic Engineering, City University of Hong Kong, Kowloon. From 1987 to 1992 he joined the Department of Electronic Engineering at the Chinese University of Hong Kong as a Lecturer. He returned to the City University of Hong Kong in January 1992 where he is presently a Professor in the Department of Electronic Engineering. He is the author of three research book chapters, 82 journal papers, and 80 conference papers. His postgraduate studies were on Gaussian beam wave theory and microwave open resonators and their applications. Currently, his research interests include design of microstrip, planar and dielectric resonator antennas, microwave measurements, computational electromagnetics, and microwave aspects of lightwave technology.

Dr. Luk is the Technical Program Chairperson of the 1997 Progress in Electromagnetics Research Sympoium (PIERS'97) and the General Vice-Chairperson of the 1997 Asia-Pacific Microwave Conference. He is a member of the Electromagnetics Academy. He received the Japan Microwave Prize at the 1994 Asia-Pacific Microwave Conference in Chiba, Japan, in December 1994. His name is included in *Who's Who in the World 1998*.